

Supplementary Materials: Three-Dimensional Surface Displacement Field Associated with the 25 April 2015 Gorkha, Nepal, Earthquake: Solution from Integrated InSAR and GPS Measurements with an Extended SISTEM Approach. Remote Sens. 2016, 8, 559; doi:10.3390/rs8070559

Haipeng Luo and Ting Chen

Table S1. Fault geometry in the synthetic tests.

Length (km)	Width (km)	Strike (°)	Dip (°)	Rake (°)	Depth* (km)
30	18	105	15	60	1

* Depth denotes the upper depth of fault plane to surface.

Table S2. Interferograms associated with the Gorkha earthquake used in this Study [1].

Track	Reference Date Product	Repeat Date Product	Model
048	22 February 2015	03 May 2015	ScanSAR
157	21 February 2015	2 May 2015	ScanSAR
047	31 March 2015	28 Apr 2015	ScanSAR

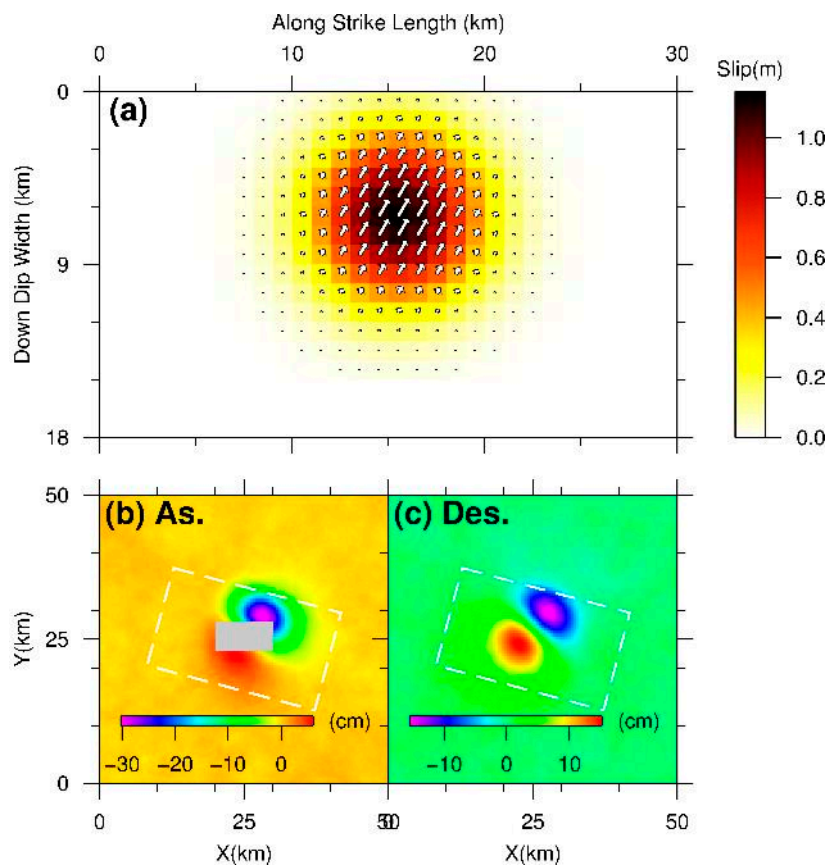


Figure S1. Fault slip distribution and InSAR LOS measurements used in the synthetic tests. (a) fault slip distribution; (b,c) show the InSAR LOS measurements of ascending and descending tracks, respectively, simulated from the true displacements shown in Figure 2; the grey region shown in (b) lacks InSAR LOS measurements.

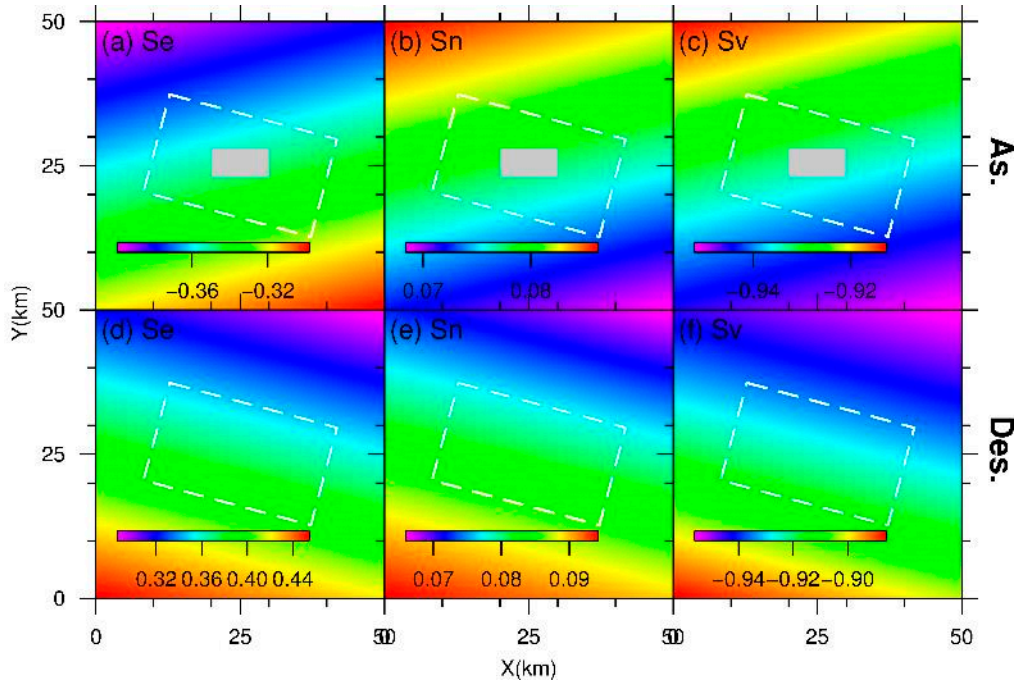


Figure S2. Unit vectors relating InSAR LOS measurements to surface displacements used in synthetic tests: (a–c) the unit vectors of ascending InSAR image in east, north and vertical directions, respectively; (d–f) the unit vectors of descending InSAR image.

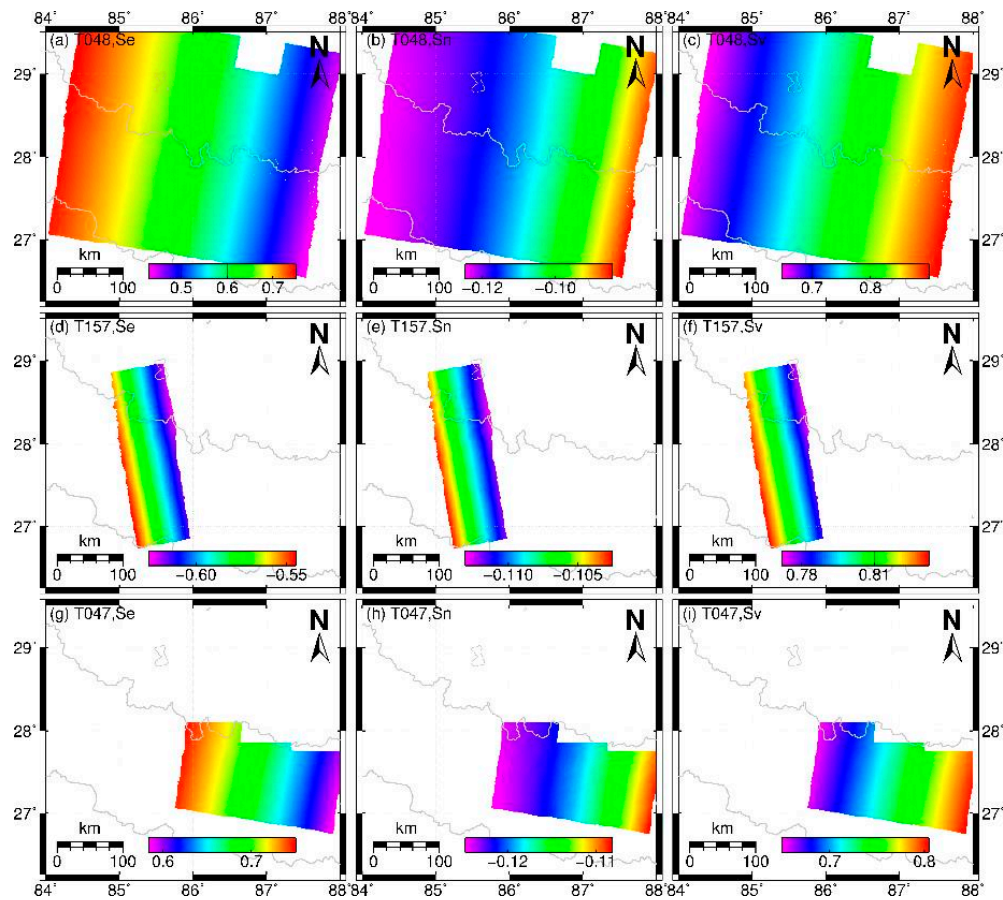


Figure S3. Unit vectors relating InSAR LOS measurements to surface displacements for the ALOS images used in the Gorkha earthquake: (a–c) the unit vectors for Track 048; (d–f) the unit vectors for Track 157; and (g–i) the unit vectors for Track 047.

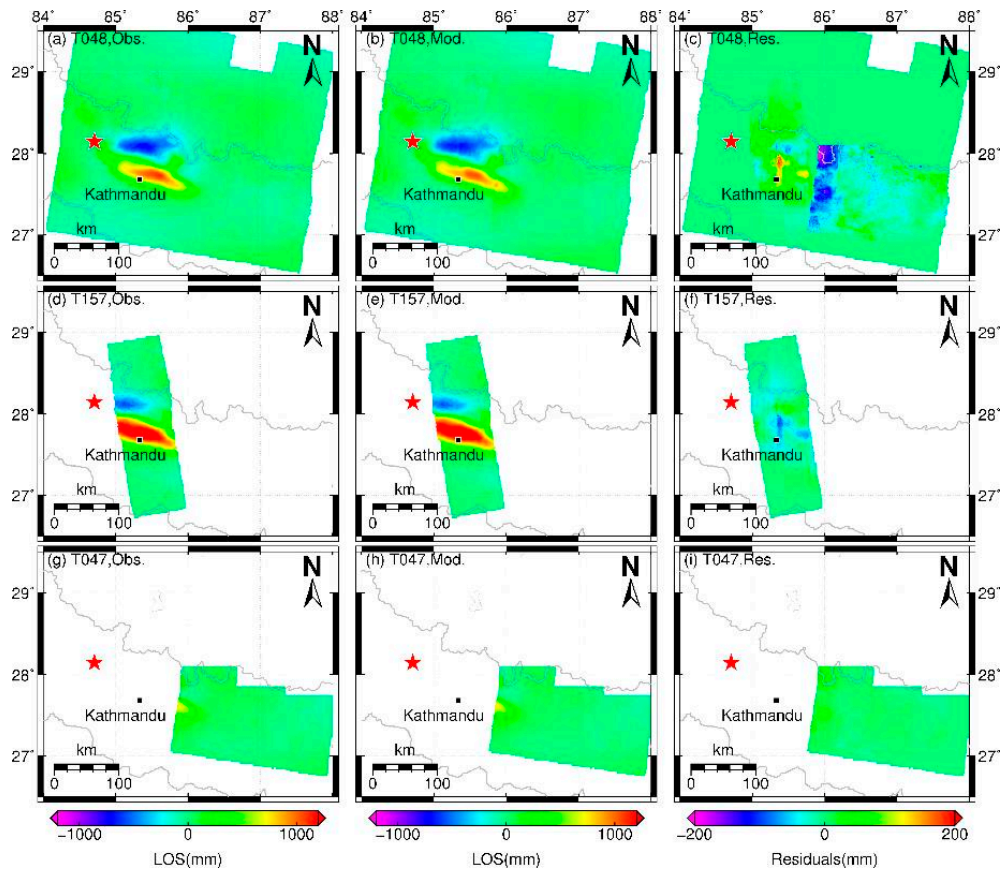


Figure S4. Comparisons of observed and modeled InSAR LOS displacements for the Gorkha earthquake: (a–c) the observed displacements; (d–f) the modeled displacements; and (g–i) the residuals.

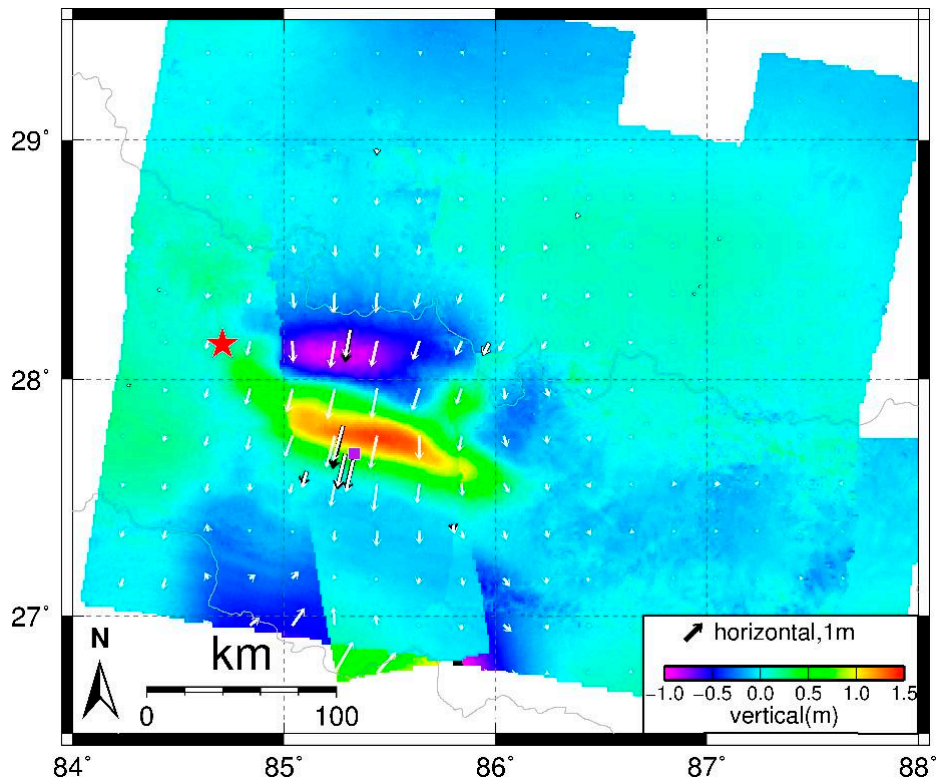


Figure S5. Three-dimensional surface displacement field due to the Gorkha earthquake modeled with SISTEM approach. White arrows show the modeled horizontal displacements and are every 20 km, and black arrows represent the GPS observations.

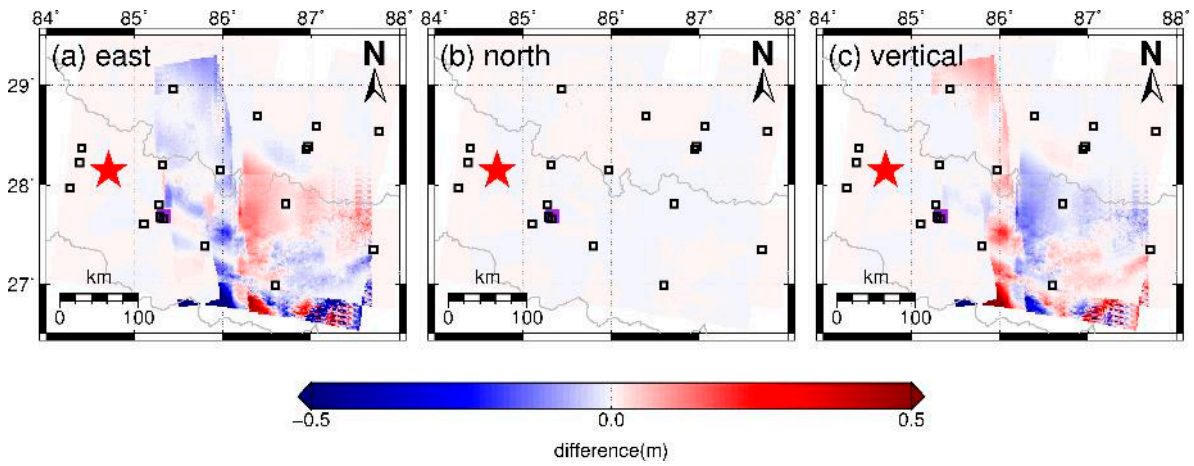


Figure S6. Differences between derived displacements with RSISTEM and SISTEM approaches: (a) east; (b) north; and (c) vertical component.

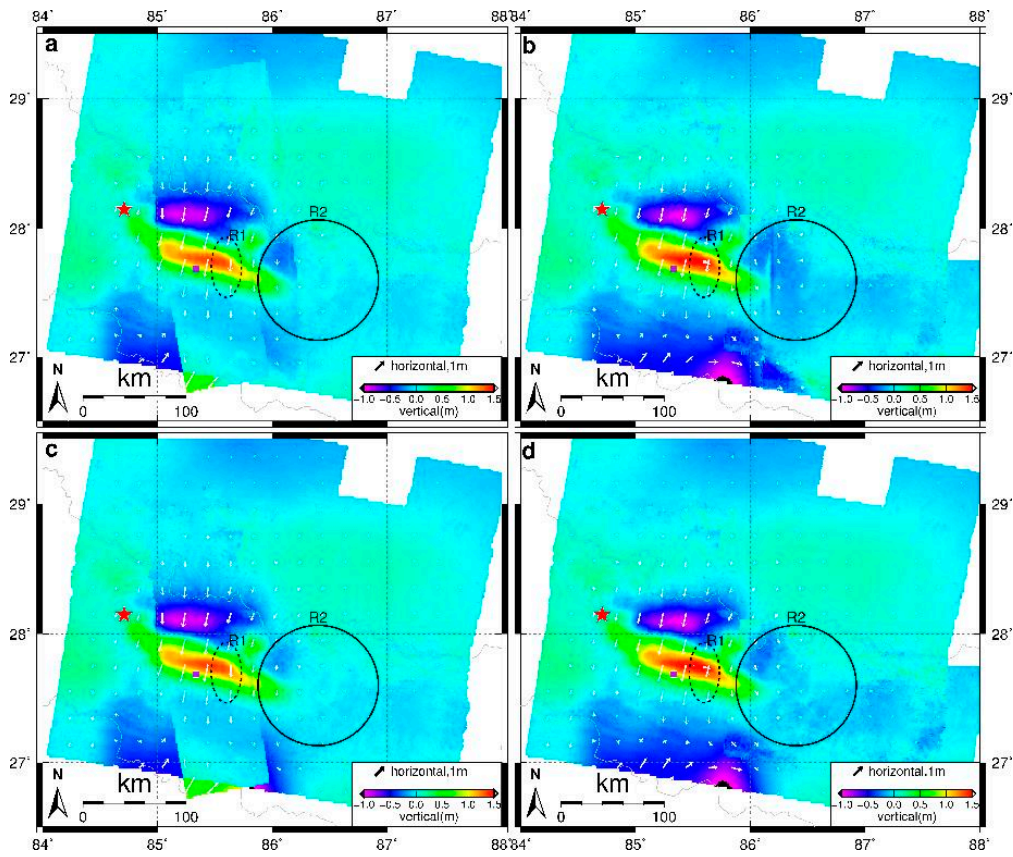


Figure S7. Comparison of solutions with different input. Top: ESISTEM-derived displacements (a) from integrated horizontal GPS observations and InSAR images of tracks 048 and 157, and (b) from integrated horizontal GPS observations and InSAR images of tracks 048 and 047. Bottom: SISTEM-derived displacements (c) from integrated horizontal GPS observations and InSAR images of tracks 048 and 157, and (d) from integrated horizontal GPS observations and InSAR images of tracks 048 and 047. Discontinuity in figures may be attributed to postseismic deformation or InSAR-related errors.

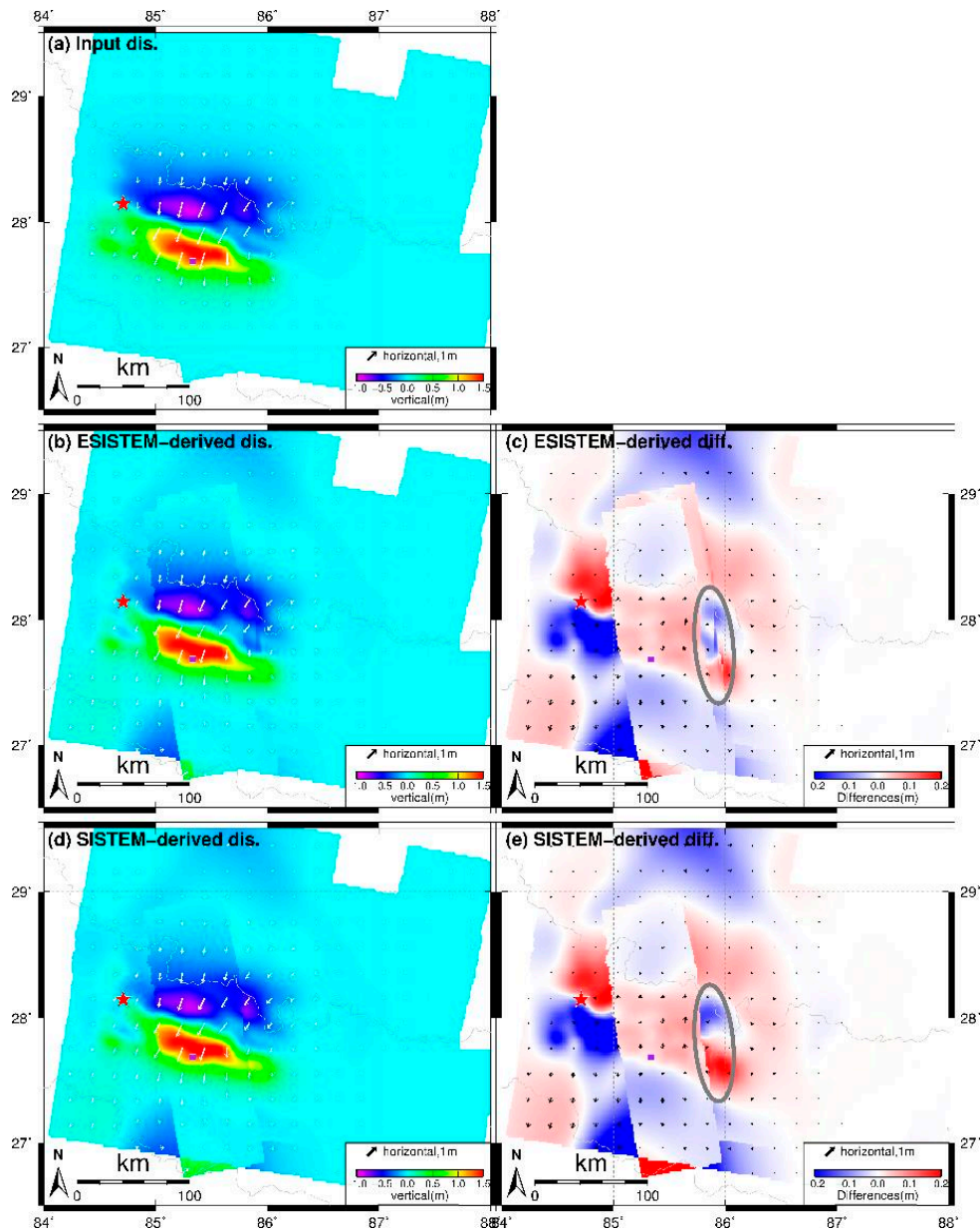


Figure S8. Model resolution test for Gorkha earthquake given data coverage. (a) input three-dimensional surface displacement field; (b) shows ESISTEM-derived displacements and (c) shows differences between ESISTEM-derived and input displacements; (d) shows SISTEM-derived displacements and (e) shows differences between SISTEM-derived and input displacements. Grey ellipses mark the region where ESISTEM-derived displacements have smaller differences to the input ones than the SISTEM-derived displacements. Model resolution test shows that that both ESISTEM and SISTEM approaches can obtain robust estimates of displacements in regions significantly deformed.

Reference

1. Lindsey, E.O.; Natsuaki, R.; Xu, X.; Shimada, M.; Hashimoto, M.; Melgar, D.; Sandwell, D.T. Line-of-sight displacement from ALOS-2 interferometry: Mw 7.8 Gorkha Earthquake and Mw 7.3 aftershock. *Geophys. Res. Lett.* **2015**, *42*, 6655–6661.

